Bioactive Materials 48 (2025) 550–563

Contents lists available at ScienceDirect

Bioactive Materials

journal homepage: www.keaipublishing.com/en/journals/bioactive-materials

# Innovative liquid embolic agents based on deep eutectic solvent: Rapid gelation in situ via solvent exchange with water for endovascular embolization

Yitong Zhou [a,b,c,1], Menghui Liu [d,1], Chuandong He [a,b], Jiayuan Lin [a,b], Yanlv Chen [a,b], Mingyu Yu [e], Yuhan Jiang [e], Xin Peng [a,b,*]

[a] Guangdong Provincial Engineering Research Center of Molecular Imaging, The Fifth Affiliated Hospital, Sun Yat-sen University, Zhuhai, 519000, PR China
[b] Guangdong-Hong Kong-Macao University Joint Laboratory of Interventional Medicine, The Fifth Affiliated Hospital, Sun Yat-sen University, Zhuhai, 519000, PR China
[c] Department of Interventional Medicine, The Fifth Affiliated Hospital, Sun Yat-sen University, Zhuhai, 519000, PR China
[d] Department of Radiology, Hunan Engineering Research Center for Intelligent Medical Imaging of Central South University, Furong Laboratory of Central South University, Molecular Imaging Research Center of Central South University, National Clinical Research Center for Geriatric Disorders, Xiangya Hospital, Central South University, Changsha, 410008, PR China
[e] Department of Orthopedics, The Fifth Affiliated Hospital, Sun Yat-sen University, Zhuhai, 519000, PR China

ARTICLE INFO

*Keywords:*
Liquid embolic agent
Deep eutectic solvent
Poly (lipoic acid) hydrogels
Solvent exchange
In situ gelation

ABSTRACT

Current liquid embolic agents face several challenges, including poor biocompatibility and vascular recanalization. Herein, we propose an innovative liquid embolic agent composed of a coenzyme-based polymer (poly lipoic acid, PLA) and a biocompatible solvent (deep eutectic solvent, DES). The agent undergoes phase transformation to form a stable hydrogel in situ through solvent exchange with water, thereby enabling safe and effective embolization. First, DES is obtained by heating a mixture of choline chloride (ChCl) and glycerol (Gly). Subsequently, lipoic acid (LA) is incorporated into the DES and heated to produce the PLA/DES complex. Owing to the strong hydrogen bonding between the DES and PLA, the DES acts as a solvent while also inhibiting PLA depolymerization. Upon contact with blood, most of the DES exchange with water, whereas some amount of ChCl integrates within the PLA via strong hydrogen bonding. This hydrogen bonding not only prevents PLA depolymerization but also reinforces the PLA network, resulting in a stable PLA hydrogel rather than depolymerized LA monomers. Furthermore, liquid-metal (LM) nanoparticles are incorporated to fabricate radiopaque PLA/LM/DES. PLA/LM/DES shows better in vitro hemocompatibility and cytocompatibility, milder inflammatory response in a rat model, and more effective and safer embolization in a rabbit model than a commercial embolic agent (Onyx). Thus, this work provides an innovative liquid embolic agent and broadens the biomedical applications of DES.

## 1. Introduction

Endovascular embolization is a minimally invasive technique used to treat hemorrhagic lesions, arteriovenous malformations, aneurysms, and solid tumors. In this procedure, embolic agents are precisely deployed to occlude diseased or injured vessels, and the therapeutic efficiency of this procedure is substantially influenced by the properties of the embolic agents [1,2]. Although solid embolic agents, such as coils, polyvinyl alcohol, and gelatin particles, offer distinct advantages in clinical settings, they are inherently limited by their fixed dimensions and shapes, which prevent them from embolizing irregular target blood vessels or distal small vessels. By contrast, liquid embolic agents exhibit unique properties, forming casts upon contact with blood and entering target blood vessels that catheters and solid embolic agents fail to reach.

Liquid embolic agents are of two types: shear-thinning and in situ–gelling agents. Oklu et al. fabricated a series of injectable hydrogels as

Peer review under the responsibility of KeAi Communications Co., Ltd.
* Corresponding author. Guangdong Provincial Engineering Research Center of Molecular Imaging, The Fifth Affiliated Hospital, Sun Yat-sen University, Zhuhai, 519000, PR China.
*E-mail address:* pengx68@mail.sysu.edu.cn (X. Peng).
[1] These authors contributed equally to this work.

https://doi.org/10.1016/j.bioactmat.2025.02.037
Received 13 December 2024; Received in revised form 4 February 2025; Accepted 23 February 2025

shear-thinning embolic agents by mixing negatively charged nanoclays with silk [3], extracellular matrix [4], lyophilized platelet-rich plasma [5], and gelatin [6]. These agents could be used as novel liquid embolic agents. Moreover, in our previous study, a coacervate prepared based on liquid−liquid phase separation was employed as a liquid embolic agent [7]. However, if the mechanical properties of shear-thinning embolic agents are too strong, their advancement through microcatheters becomes challenging. Conversely, if the mechanical properties are too weak, they are at a risk of being washed away by the blood, leading to vascular recanalization. In situ-gelling agents can undergo gelation in situ by solvent exchange, pH, temperature, or light; metal ions have also been used for endovascular embolization [1,8–11]. For instance, commercial liquid embolic agents (Onyx and PHIL) consist of a polymer and dimethyl sulfoxide (DMSO), which undergo solvent exchange upon contact with blood to form a precipitate in situ, resulting in embolization [1]. Zhang and co-workers utilized mildly acidic stimuli to trigger the welding of microgels within aneurysms, achieving complete embolization [9]. However, DMSO and acidic solutions typically induce vasospasm or vasoconstriction [12,13]. Furthermore, Duan et al. reported a temperature-sensitive poloxamer 407 (F127)/hydroxymethyl cellulose (HPMC)/sodium alginate (SA)-derived hydrogel, which undergoes a sensitive phase transition in blood vessels to achieve embolization [10]. However, thermosensitive embolic agents tend to gel inside long catheters, leading to their occlusion. Kim and co-workers reported a liquid embolic agent based on an in situ formed double-crosslinked alginate--based hydrogel that was triggered by harmless visible-light irradiation and $Ca^{2+}$ in the blood [11]. However, using a light source for tiger gelation requires specialized catheters, which can increase the cost and complexity of the operation. Overall, current in situ gelling systems are either unfriendly to vascular walls, difficult to operate, or costly. Therefore, new liquid embolic agents satisfying clinical requirements must be developed.

Deep eutectic solvent (DES), which are defined as mixtures of hydrogen-bond donors and acceptors with melting points below room temperature, are emerging as ecofriendly alternatives to conventional organic solvents [14]. Their exceptional solubilization properties, biocompatibility, environmental sustainability, and versatility are driving a surge in their applications in pharmaceutical and biomedical fields. The solubilization capacity of DES is profoundly influenced by their structural characteristics, particularly the identities of their hydrogen-bond donors and acceptors. For example, DESs formulated from choline chloride (ChCl) and various polyols (such as glycerol [Gly] or ethylene glycol) exhibit enhanced solubility in active pharmaceutical ingredients, which can be attributed to the formation of strong intermolecular interactions and the ability to establish a conducive microenvironment for solute dissolution [15]. This solubilization phenomenon can be further optimized by selecting DES components with shorter alkyl chains and polar, nonaromatic characteristics, enhancing selectivity and the capacity to solubilize compounds such as quinine and clozapine [16]. Furthermore, the application of theoretical models, such as COSMO-RS, combined with machine learning techniques, aids in improving our understanding of the solubility landscape and enables the rational design of DES specific for pharmaceutical applications, thereby unlocking new pathways for drug formulation and delivery [15–21]. Liquid embolic agents derived from DESs have been introduced recently. Oklu et al. reported a liquid embolic material composed of polyethylene glycol (PEG) and a biocompatible ionic liquid for rapid microvessel embolization to treat small-vessel hemorrhages.

Lipoic acid (LA), an essential coenzyme in animals, undergoes thermal ring-opening polymerization (ROP) to form its metastable polymer polylipoic acid (PLA), which undergoes spontaneous inverse ring-closing depolymerization initiated by terminal reactive radicals [22]. Furthermore, PLA dissolves well in organic solvents while exhibiting only limited solubility in water. This makes it a promising candidate for the development of solvent exchange-based liquid embolic agents. However, PLA prepared in conventional organic solvents is metastable, causing its depolymerization to semicrystalline PLA oligomers or LA monomers following solvent exchange with water. Furthermore, the Galinstan liquid metal (LM), characterized by excellent biocompatibility and fluidity, was used as a contract agent to monitor the position of this liquid embolic agent during operation.

In this study, we developed an innovative liquid embolic agent comprising DES and PLA. DES not only functions as a solvent but also plays a critical role in preventing the depolymerization of PLA. This dual functionality facilitates the formation of a stable PLA hydrogel after solvent exchange with water, thus ensuring effective embolization. First, DES was obtained by heating a mixture of ChCl and Gly. Subsequently, LA powder was added to the DES and heated to synthesize PLA. ChCl forms strong hydrogen bonding with the carboxylic acid groups in PLA, thus preventing its depolymerization. Upon contact with water, most of the DES was replaced by water molecules, whereas some amount of ChCl remained integrated within the PLA by means of the strong hydrogen bonding. Thus, instead of depolymerized LA monomers, a stable PLA hydrogel was formed. Furthermore, Galinstan LM nanoparticles (NPs) were introduced to prepare radiopaque PLA/LM/DES, allowing the monitoring of the liquid embolic agent's position during the operation. Moreover, the mechanical properties, hemocompatibility, cytocompatibility, and in vivo biocompatibility of the PLA/LM/DES solution was compared with those of a commercial liquid embolic agent (Onyx). Finally, the embolization performance of the PLA/LM/DES solution and Onyx in the renal artery and ruptured femoral artery molds of rabbits was further studied. Owing to its easy preparation, desirable biocompatibility, and effective embolization performance, the PLA/LM/DES liquid embolic agent may be a promising next-generation liquid embolic agent for endovascular embolization (Fig. 1).

## 2. Materials and methods

### 2.1. Materials

ChCl, Gly, LA and DMSO were purchased from Aladdin, China. Galinstan LM was procured from Dongguan Chingming Metal Technology Co., Ltd., China. Iohexol contrast agent (300 mg/mL) was purchased from Jiangsu Hengrui Medicine Co., Ltd., China. Onyx was bought from Micro Therapeutics Inc. company, US, and glycerol assay kits and live/dead cell staining kits were purchased from Beyotime (Shanghai, China).

### 2.2. Preparation

DES was prepared by heating ChCl and Gly at different molar ratios at 80 °C for 8 h. The LA powder was then added into DES, and the samples were heated at 99 °C for 12 h. Among all samples, we found that the one with a ratio of 1:3 (ChCl: Gly) exhibited the highest solubility (0.2 g/mL) for PLA. Dissolving more PLA can facilitate rapid embolization; therefore, we chose this ratio. Accordingly, 0.4 g LA powder was dissolved into 2 mL DES, and the samples were heated at 99 °C for 12 h. Meanwhile, LM was ultrasonicated (1800 W) in DES (1.27 g/mL) for 20 min to prepare LM NPs. PLA/DES and LM/DES were then mixed to obtain the PLA/LM/DES solution. Finally, PLA/DES and PLA/LM/DES were introduced into water to obtain the PLA and PLA/LM hydrogels. Simultaneously, 0.4 g LA powder was dissolved in 2 mL DMSO, and the samples were heated at 99 °C for 12 h. The PLA/DMSO solution was then introduced into water to obtain PLA hydrates. Because DES and their constituent components are highly hygroscopic, we ensured that these samples were maintained in a sealed container throughout preparation and storage.

### 2.3. Characterization

The LA powder, dried PLA gel, and PLA/DMSO hydrates were analyzed using a Raman spectrometer (Horiba LabRAM HR, Japan) at an excitation wavelength of 785 nm and subjected to X-Ray diffraction

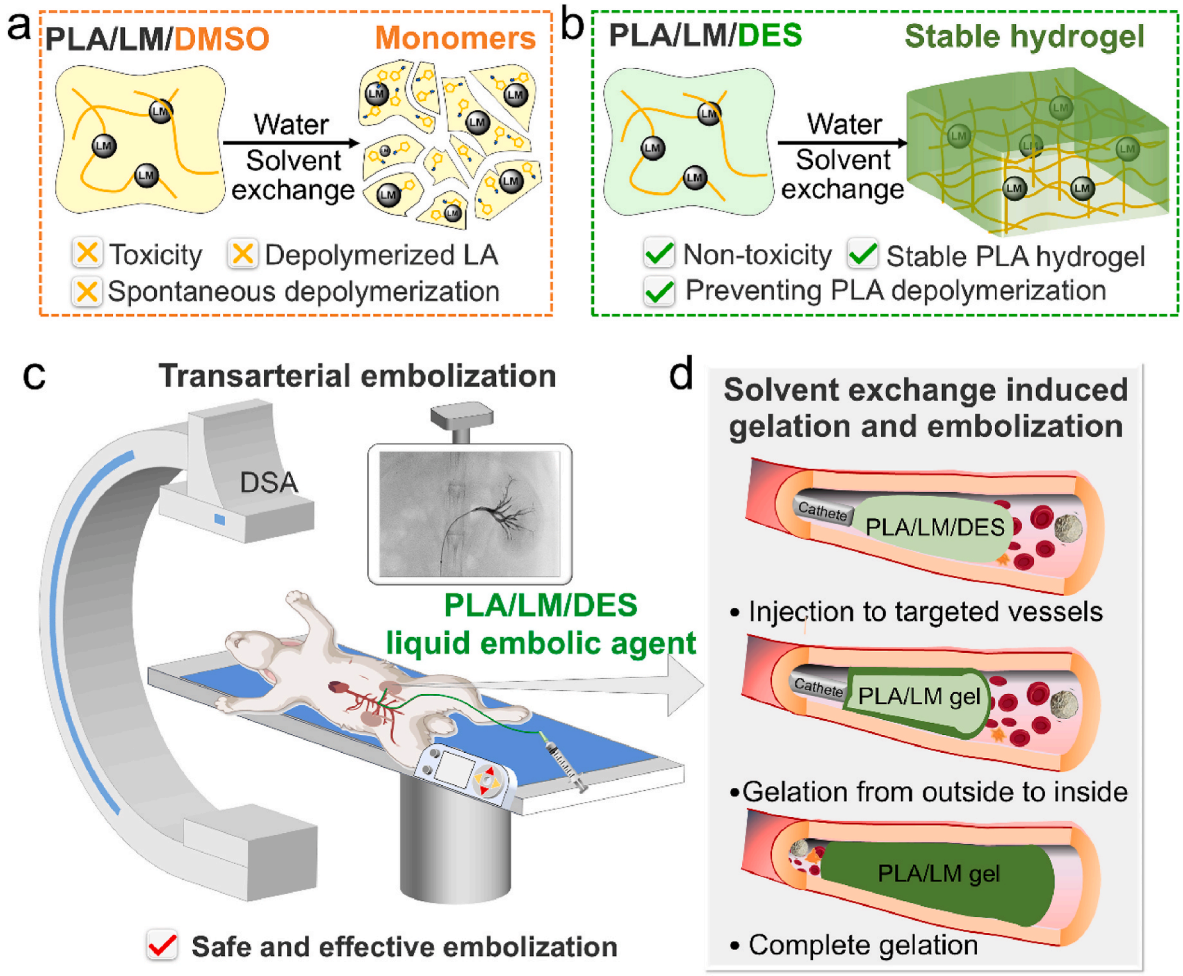


**Fig. 1.** (a) Schematic of the depolymerization of PLA/LM/DMSO upon solvent exchange with water. (b) Schematic of the transformation of PLA/LM/DES to stable a PLA/LM hydrogel upon solvent exchange with water. (c) Schematic of transarterial embolization in a rabbit. (d) Schematic of solvent exchange–induced gelation of PLA/LM/DES and its embolization in a blood vessel.

(XRD). Subsequently, the dried PLA gel and PLA/DMSO hydrates were observed using a scanning electron microscope, and Fourier-transform infrared (FTIR) spectroscopy (Thermo Scientific Nicolet iS10, USA) was used to characterize LA, ChCl, ChCl + LA, Gly, DES, PLA gel, and PLA/LM gel. UV–Vis spectroscopy (PerkinElmer, Inc., Waltham, MA, USA) was used to characterize DES, PLA, and PLA/DES. The PLA/LM gel was characterized using X-ray photoelectron spectroscopy (XPS; Axis Ultra, Kratos, UK). All dried PLA/LM gel were prepared by freeze-drying. The radiopacity and CT value of PLA/LM/DES containing various LM NPs were evaluated using CT scanning.

### 2.4. Gelation time test

A total of 0.4 mL PLA/LM/DES was deposited into a centrifuge tube (contact area = 1.8 $cm^2$) and beaker (contact area = 15.8 $cm^2$), and 5 mL SGF was added and incubated at 37 °C. At a pre-set time, the centrifuge tube and beaker were inverted to observe the fluidity of the samples. The solidification time was recorded as complete gelation time.

### 2.5. Injectability test

A syringe containing the PLA/LM/DES solution connected to different microcatheters was loaded and fixed on an electronic universal testing machine (MTS, C42.503, USA). The solution was pushed at a flow rate of 1 mL/min, and the force was recorded. The experiment was performed in triplicate to ensure data reliability.

### 2.6. Mechanical tests

An MCR 92 rheometer (Anton Paar, Austria) and a parallel plate system (diameter = 25 mm) were used to test the rheological properties of the samples at 37 °C. Time oscillatory sweeps were performed at constant strain (1 %) and angular frequency ($\omega$ = 10 rad/s). The electronic universal testing machine was used to test the tensile properties of the samples. Dumbbell-shaped hydrogels specimens with a thickness of 2 mm (standardized as DIN-53504 S3 with an overall length of 35 mm, width of 6 mm, inner width of 2 mm, and gauge length of 10 mm) and a crosshead speed of 10 mm/min were used as samples. Tensile strain was defined as the change in the length relative to the initial length. Tensile stress was calculated as $F/ab$ ($a$ and $b$ are the initial thickness and width of the specimen, respectively). To ensure data reliability, the experiment was performed three times.

### 2.7. Hemolysis test

Rabbit erythrocytes were collected from whole blood by centrifugation (200×$g$, 10 min) and diluted to 5 % (v/v) with physiological saline. To 1 mL of diluted erythrocyte solution, 100 μL PLA/LM/DES solution, 100 μL Onyx, or 100 mg PLA/LM hydrogel was added, and they were coincubated at 37 °C. Negative group: physiological saline solution; positive group: deionized water. After 24 h, the erythrocyte suspensions were centrifuged at 500×$g$ for 5 min, and the absorbance ($A$) of the supernatants were measured at 540 nm to calculate hemolysis ratio,

given by the following formula.

$$\text{Hemolysis ratio } (\%) = (A_s - A_p) \ / \ (A_d - A_p) \times 100\%$$

Here, $A_s$, $A_p$, and $A_d$ represent the absorbance of samples, physiological saline, and water, respectively. The experiment was performed in triplicate to ensure data reliability.

### 2.8. In vitro biocompatibility and degradation tests

Human umbilical vein endothelial cells (HUVECs) were added to plates and cultured at 37 °C for 12 h (density = $2.5 \times 10^4$ cells per well). Thereafter, 100 μL PLA/LM/DES solution, 100 μL Onyx, or 100 mg PLA/LM hydrogel were added to HUVECs. Positive group: pure growth medium. After 24 h, the live/dead cell staining method was used to assess cell viability. PLA/LM hydrogels were soaked in simulated physiological fluid at 37 °C, and their dried weight was recorded at pre-set time to calculate degradation ratio per the following formula.

$$\text{Degradation ratio } (\%) = (m_0 - m_1) \ / \ m_0 \times 100\%$$

Here, $m_1$ and $m_0$ represent the remaining and initial mass of the dried hydrogels, respectively.

### 2.9. In vivo biocompatibility and degradation tests

All the experiments complied with the animal ethics guidelines of the Animal Ethics Committee of the Fifth Affiliated Hospital of Sun Yat-sen University (00551). Male Wistar rats (6–8 weeks of age) were purchased from Guangzhou Jin Wei Biotechnology Co., Ltd. and acclimated to the environment for one week. After anesthesia, 300 μL PLA/LM/DES or Onyx were injected into the dorsal subcutaneous tissue of rats. At a preset time, whole blood was collected for routine blood and serum biochemistry tests. On days 14 and 28, the hydrogels were collected to determine their in vivo degradation ratios. The tissues surrounding the hydrogels were collected, fixed, dehydrated, and embedded in paraffin.

### 2.10. Renal artery embolization in a rabbit model

All the experiments complied with the animal ethics guidelines of the Animal Ethics Committee of the Fifth Affiliated Hospital of Sun Yat-sen University (IAC24W123). Rabbits (2.4–3.0 kg, male) were purchased from Zhuhai Bestest Biotechnology Co., Ltd. and acclimated to the environment for one week. Anesthesia was induced with Zoletil 50 (5 mg/kg, intramuscular injection) and 2 % xylazine (2 mg/kg, intramuscular injection). First, we dissected and suspended the femoral artery (FA) and made an incision (diameter = 0.1 mm) on it. Thereafter, a 2.7 F microcatheter (SL 10, Stryker, USA) was inserted into the FA through the incision and advanced to the right renal artery via the abdominal aorta under real-time X-ray fluoroscopy guidance using a digital subtraction angiography (DSA) machine (Allura Xper FD20, Philips, Netherlands). After that, iohexol (0.2–0.4 mL) was employed to confirm the patency of the renal artery. Subsequently, 0.1–0.2 mL of the PLA/LM/DES solution or Onyx was slowly deployed to embolize the renal artery via a microcatheter with a real-time X-ray fluoroscopy monitor. Computed tomography (CT) (Brilliance 16 row, Philips, Netherlands) was performed to confirm embolization of the renal artery. Simultaneously, blood was collected and tested for glycerol levels from 0 to 3.5 h. On days 14 and 28, the rabbits were re-examined using CT, color Doppler flow imaging (CDFI), and contrast-enhanced ultrasound (CEUS). The rabbits were euthanized, and the embolized renal arteries and kidneys were collected, fixed in phosphate-buffered formalin, dehydrated, and embedded in paraffin.

### 2.11. Ruptured femoral artery embolization in a rabbit model

After dissection and suspension, an incision was made in the carotid artery (diameter = 0.1 mm) using microscissors. A 2.7 F microcatheter was inserted into the carotid artery through the incision and advanced to the femoral artery (FA) via the abdominal aorta. After puncturing the FA to induce bleeding, PLA/LM/DES or Onyx (0.2–0.3 mL) was slowly deployed into the ruptured FA to stop bleeding. The weight of lost blood was recorded, and the blood was tested for glycerol levels from 0 to 3.5 h. On days 1 and 7 after treatment, the rabbits were reexamined by using CT, CDFI, and CEUS. The rabbits were euthanized, and the femoral arteries were collected and fixed in phosphate-buffered formalin, dehydrated, and embedded in paraffin.

### 2.12. Hematoxylin & eosin (H&E) and Masson's staining

All slides were baked at 60 °C for 10 min, deparaffinized with xylene and gradient ethanol, and rehydrated in deionized water. The slides were stained with H&E and Masson's staining kit according to the manufacturer's instructions. All stained slides were scanned using the Case Viewer software (3DHISTECH Ltd., Hungary).

### 2.13. Statistical analysis

Statistical analyses were executed in GraphPad Prism version 10. Data are presented as mean ± standard deviation (SD). Comparative assessments of the experimental datasets were performed using Student's *t*-test for two-group comparisons and one-way ANOVA for multiple groups, complemented by Tukey's post-hoc test for detailed intergroup significance. Statistical significance levels are denoted as ns, $p > 0.5$, $^*p < 0.05$, $^{**}p < 0.01$, $^{***}p < 0.001$, and $^{****}p < 0.0001$.

## 3. Results

### 3.1. Preparation and properties of the PLA/DMSO and PLA/DES and their derived hydrates

Upon heating, LA underwent ROP to form metastable PLA, which spontaneously depolymerized to yield LA monomers (Fig. 2a). First, a conventional organic solvent, dimethyl sulfoxide (DMSO) was used. LA was added to DMSO and heated, resulting in the formation of a PLA/DMSO solution in which DMSO formed weak hydrogen bonding with the carboxylic acid (–COOH) groups of PLA. Upon introducing PLA/DMSO into water, DMSO was fully replaced by water molecules, resulting in the formation of a metastable PLA/$H_2O$ complex. Subsequently, the metastable PLA spontaneously depolymerized to yield LA monomers in water (Fig. 2c). Second, by heating Gly, a hydrogen bond donor, and ChCl, a hydrogen bond acceptor, at 80 °C for 8 h, DES was formed because of strong hydrogen bonding (Fig. 2b) [23–25]. Subsequently, LA powder was added to DES and heated at 99 °C for 12 h to form PLA/DES. In this system, the DES could form strong hydrogen bonding with PLA, which prevents PLA depolymerization [26,27]. The hydrogen bonding between the components were characterized using FTIR and UV–Vis spectroscopy. In the FTIR spectra, the hydroxyl group (–OH) peaks of Gly (3282 $cm^{-1}$) and ChCl (3252 $cm^{-1}$) shifted to 3299 $cm^{-1}$ in the DES, indicating hydrogen bonding between Gly and ChCl. The –OH peaks in the DES (3299 $cm^{-1}$) and PLA gel (3325 $cm^{-1}$) shifted to 3304 $cm^{-1}$ in the PLA/DES, indicating hydrogen bonding between them (Fig. S1 and Table S1). Moreover, in UV–Vis spectroscopy, the absorption peaks of Gly (253 nm) and ChCl (252 nm) shifted to 255 nm in the DES, and those of DES (255 nm) and PLA gel (259 and 309 nm) shifted to 266 and 335 nm in the PLA/DES, respectively (Fig. S2) [28,29]. Thus, these results indicated hydrogen bonding between PLA and DES.

After the introduction of PLA/DES into water, most of the DES was replaced with water molecules, whereas some ChCl remained integrated within the PLA via strong hydrogen bonding. This hydrogen bonding prevented PLA depolymerization and enhanced the PLA network, resulting in the formation of a stable PLA hydrogel capable of stretching (Fig. 2d). After immersion in water for one week, the PLA hydrogel

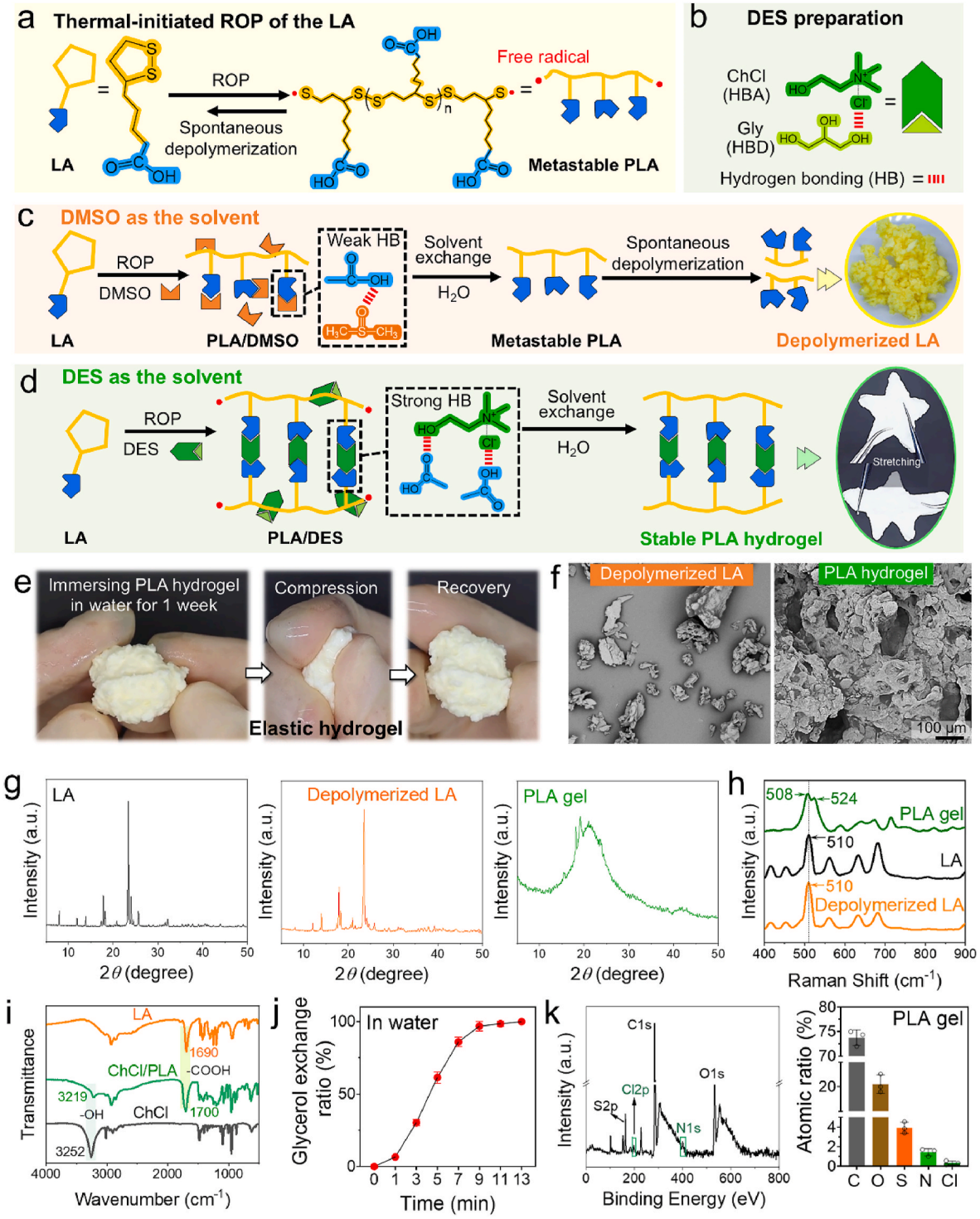


**Fig. 2.** Preparation and properties of PLA/DMSO and PLA/DES and their derived hydrates. (a) Schematic of the ROP of LA and spontaneous depolymerization of metastable PLA. (b) Schematic of DES formation of. (c) Schematic of LA polymerization in DMSO and PLA depolymerization upon solvent exchange with water. (d) Schematic of LA polymerization in DES and the transformation of PLA/DES to PLA hydrogel upon solvent exchange with water. (e) Elastic PLA hydrogel after immersion in water for one week. (f) SEM images of the depolymerized LA monomers and PLA hydrogel. (g, h) XRD (g) and Raman (h) spectra of the LA powder, depolymerized LA monomers, and PLA gel. (i) Fourier transform infrared (FTIR) spectra of LA, ChCl, and their complex. (j) Glycerol exchange ratio of PLA/LM/DES in deionized water. (k) XPS and atomic ratio of the final PLA gel. Gly: glycerol; ChCl: choline chloride; DES: deep eutectic solvent; LA: lipoic acid; PLA: poly (lipoic acid). Data are shown as the mean ± SD.

maintained good elasticity (Fig. 2e). Moreover, scanning electron microscopic images revealed that the dried PLA oligomers exhibited a dispersed granular morphology, whereas the PLA gel showed a continuous structure containing pores (Fig. 2f).

The PLA/DMSO and PLA/DES-derived hydrates were studied using XRD. LA powder and depolymerized LA monomers derived from PLA/DMSO exhibited sharp crystalline peaks, further indicating that the PLA/DMSO-derived hydrates were unstable. However, for the PLA/DES-derived hydrates, the crystallization peaks of pristine LA disappeared completely, suggesting that DES can stabilize PLA and prevent its

depolymerization (Fig. 2g). The samples were analyzed using Raman spectroscopy. LA powder and depolymerized LA monomers exhibited a disulfide bond (S−S) at 510 $cm^{-1}$, whereas the PLA gel showed two new peaks at 508 and 524 $cm^{-1}$, highlighting the unstable PLA in PLA/DMSO-derived hydrates and stable PLA in PLA/DES-derived hydrates (Fig. 2h). Moreover, the FTIR spectra of LA, ChCl, and PLA/ChCl complex exhibited that the hydroxyl peak at 3252 $cm^{-1}$ in ChCl shifted to 3219 $cm^{-1}$ in complex and carboxylic acid peaks at 1690 $cm^{-1}$ in LA shifted to 1700 $cm^{-1}$ in PLA/ChCl complex, suggesting strong hydrogen bonding between LA and ChCl (Fig. 2i and Table S1). Finally, the final

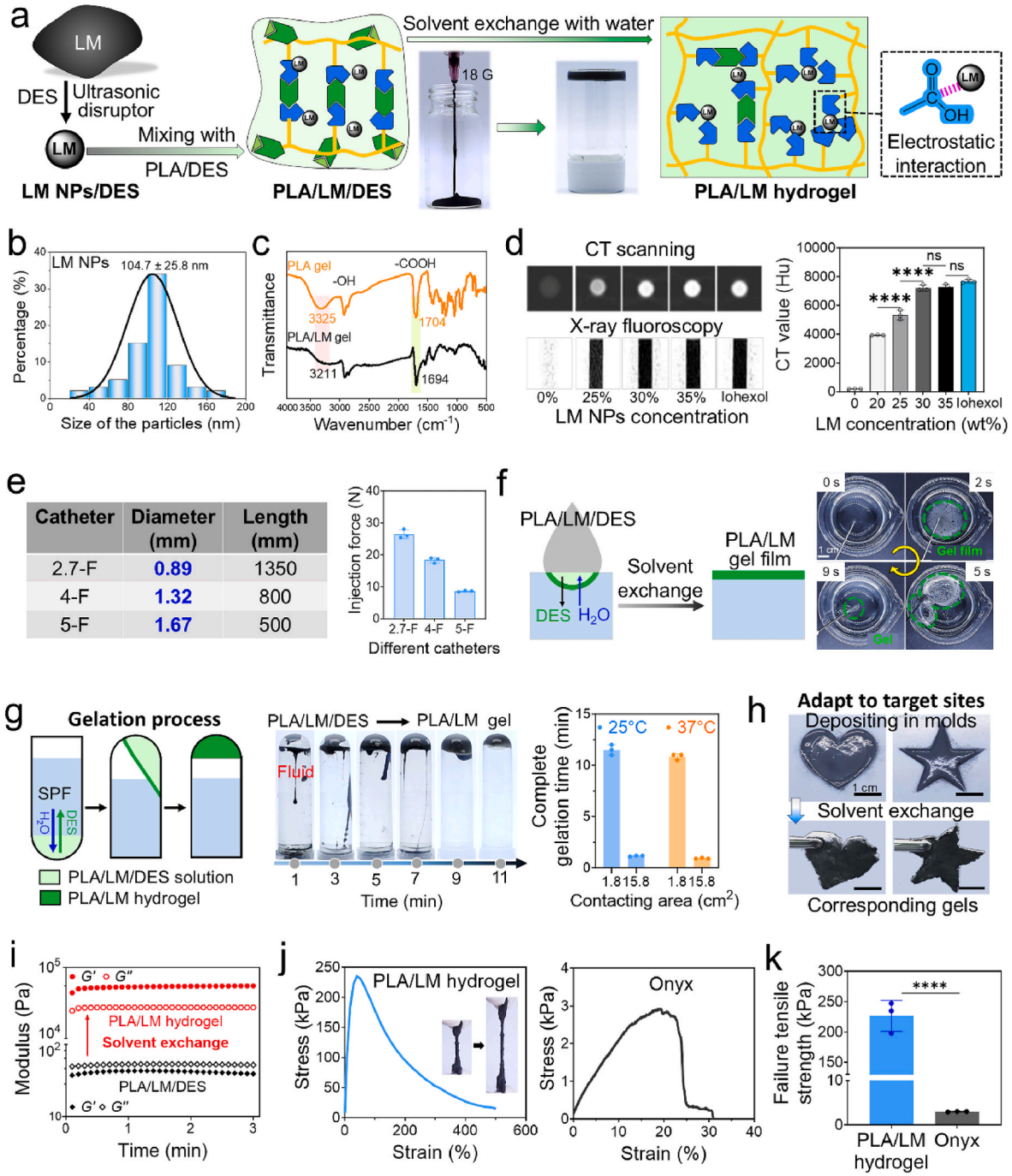


**Fig. 3.** Preparation and properties of the PLA/LM/DES liquid embolic agent and its derived PLA/LM hydrogel. (a) Schematic for the preparation of PLA/LM/DES solution and its derived PLA/LM hydrogel. (b) Size distribution of the LM nanoparticles. (c) Fourier transform infrared (FTIR) spectra of the PLA gel and PLA/LM gel. (d) CT scanning and X-ray fluoroscopy images (left) and CT values (Hu) (right) of the PLA/LM/DES solution with varying content of LM NPs. (e) Parameters of the microcatheters (left) and injection force of the PLA/LM/DES solutions that are delivered with varying microcatheters (right). (f) Gelation process of a droplet of PLA/LM/DES in water. (g) Gelation process of the PLA/LM/DES solution in a centrifuge tube (left) and complete gelation time of the PLA/LM/DES in centrifuge tube (contacting area = 1.8 $cm^2$) and beaker (contacting area = 15.8 $cm^2$) at 25 and 37 °C (right). ($n$ = 3) (h) Fabrication of the hydrogel with different shapes by depositing them in different models. (i) Time oscillatory sweeps of PLA/LM/DES solution and PLA/LM hydrogel. (j) Tensile stress–strain curves of the PLA/LM hydrogel or Onyx-derived sample that prepared by immersing PLA/LM/DES or Onyx, respectively in SPF for 2 h at 37 °C. (k) Failure tensile strength of the PLA/LM hydrogel and Onyx-derived samples. Data are shown as the mean ± SD. Statistical significance was analyzed with one-way ANOVA. ns, not significant, *$p < 0.05$, ****$p < 0.0001$.

chemical compositions of the PLA hydrogels were investigated. The PLA/LM/DES solution was immersed in deionized water, and the released glycerol content was tested using a glycerol kit. In the first 7 min, 86.0 ± 3.2 % glycerol was released, and nearly all the remaining glycerol released in the next 2 min. Thus, nearly no glycerol was present in the final PLA/LM hydrogel (Fig. 2j). XPS was employed to test the final gel, and the contents of the nitrogen (N) and chlorine (Cl) were 1.4 ± 0.4 % and 0.3 ± 0.2 %, respectively, indicating the presence of a few ChCl that remained in the final PLA/LM hydrogel (Fig. 2k). Thus, during the solvent exchange process, most DES was replaced with water molecules; however, a few ChCl molecules remained integrated in PLA through strong hydrogen bonding to prevent PLA depolymerization, resulting in a stable PLA hydrogel.

### 3.2. Preparation and properties of the PLA/LM/DES liquid embolic agent and its derived PLA/LM hydrogel

Galinstan LM was used as a contrast agent to monitor the position of the liquid embolic agent during operation. Using an ultrasonic disruptor, LM was transformed into LM NPs in DES, which were further mixed with PLA/DES to prepare radiopaque PLA/LM/DES (Fig. 3a and b). Meanwhile, the LM NPs formed electrostatic interactions with the carboxyl groups in the PLA, as indicated by the shifted characteristic peaks in the FTIR spectra (Fig. 3c). First, we assessed the fundamental characteristics of the PLA/LM/DES solution to evaluate its potential as a liquid embolic agent. For CT scanning and X-ray fluoroscopy images, the PLA/LM/DES solution containing 30 wt% LM NPs exhibited excellent X-ray radiopacity, which could be clearly identified during the operation (Fig. 3d). Moreover, the injection force of the PLA/LM/DES solution delivered using narrow and long microcatheters with different diameters was tested (Fig. 3e and S3). The injection forces of the PLA/LM/DES solution in 2.7, 4, and 5 F microcatheters were 26.5 ± 1.4, 18.4 ± 0.8, and 8.6 ± 0.2 N, respectively, which were lower than 50 N, indicating that the PLA/LM/DES solution can easily be delivered via microcatheter [30].

Next, the solvent exchange-induced gelation of the PLA/LM/DES solution was studied. Dropping a drop of the PLA/LM/DES solution into a simulated physiological fluid (SPF), the solution instantly spread on the water and underwent solvent exchange to form a hydrogel film within several seconds. This indicated that the surface of the PLA/LM/DES solution can instantly gel upon contact with water (Fig. 3f). Thereafter, the complete gelation time of the PLA/LM/DES solution was studied using the vial inversion method at 37 °C (Fig. 3g). The flow performance of the sample in the centrifuge tube gradually weakened until it reached a nonflowing hydrogel state, which was considered the complete gelation time. This process also indicated that the gelation of the PLA/LM/DES solution occurred from the outer layer to the inside via gradual solvent exchange, which allowed PLA/LM/DES to be pushed forward into the small branches via blood pressure and injection force. Moreover, to investigate the influence of contact area and temperature on the complete gelation time, we added 5 mL and 50 mL of SPF into a centrifuge tube (contact area = 1.8 $cm^2$) and beaker (contact area = 15.8 $cm^2$) containing 0.4 mL of PLA/LM/DES solution and then inversed the centrifuge tube and beaker at pre-set times. The complete gelation time was shortened with increasing contact area, whereas the temperature had no effect on the complete gelation time. In addition, the PLA/LM/DES solution can be deposited into molds with different shapes to prepare PLA/LM hydrogels with corresponding shapes, demonstrating that the PLA/LM/DES-derived hydrogel can fit the target sites with irregular shapes (Fig. 3h). The rheological properties of PLA/LM/DES solution and PLA/LM hydrogels are shown in Fig. 3i. The loss modulus ($G''$, 52.4 ± 1.0 Pa) of PLA/LM/DES solutions was higher than their storage modulus ($G'$, 41.4 ± 1.5 Pa), indicating their liquid-like characteristics. The $G'$ (53350 ± 2174 Pa) of PLA/LM hydrogels was higher than their $G''$ (27334 ± 528 Pa), indicating their elastomer-like characteristics. Finally, the mechanical properties of the PLA/LM hydrogels and commercial liquid embolic agent Onyx-derived samples were compared (Fig. 3j and k and S4). The PLA/LM hydrogels exhibited higher failure tensile strength (226.9 ± 25.6 kPa) and failure tensile strain (529.0 ± 31.0 %) than those of the Onyx-derived samples (3.0 ± 0.1 kPa and 30.9 ± 4.9 %). These better mechanical properties of the PLA/LM hydrogels indicated that they can effectively resist blood pressure without breaking during embolization.

### 3.3. Biocompatibility and biodegradability of PLA/LM/DES and its-derived PLA/LM hydrogel

We first evaluated the hemocompatibility of the PLA/LM/DES solution and PLA/LM hydrogel, which was an important parameter for embolic agents, using a hemolysis assay. Co-incubating the erythrocyte suspensions with different samples at 37 °C for 24 h, the supernatant in DES, PLA/LM/DES solution and PLA/LM gel groups exhibited a similar extent of transparency to that of the saline group, and their hemolysis ratios were lower than 5 %, indicating their excellent hemocompatibility. The hemolysis ratio of the commercial embolic agent (Onyx) was approximately 10 %, owing to the presence of DMSO (Fig. 4a). Moreover, the viability of the human umbilical vein endothelial cells (HUVEC) after coincubation with the DES, PLA/LM/DES solution, or PLA/LM hydrogel was higher than 98 %, with no statistical difference from that of the blank control group, and the cells stained green with calcein/acetoxymethyl ester (Calcein/AM) exhibited a spindle-like morphology. However, cell viability in the Onyx group was lower than 96 % (Fig. 4b). These results indicated better hemocompatibility and cytocompatibility of DES, PLA/LM/DES solution, and PLA/LM hydrogel than those of Onyx.

To compare the in vivo biocompatibility and biodegradability of the PLA/LM hydrogel and Onyx, the samples were directly injected into the dorsal subcutaneous tissues of rats (Fig. 4c). On days 14 and 24, blood was collected from the rats for blood routine and serum biochemical analyses. No significant differences were observed in blood routine (red blood cell, white blood cell, and platelet concentrations) or serum biochemical analyses (total protein, albumin, alanine aminotransferase, aspartate aminotransferase, creatinine, and urea nitrogen concentrations) between the normal rats and rats implanted with PLA/LM/DES solution and Onyx, indicating that these samples did not cause systemic inflammatory response syndrome (Fig. 4d and e). Second, PLA/LM hydrogels degraded 25.2 ± 1.0 % in SPF at 20 weeks and 10.0 ± 0.6 % in vivo at four weeks after implantation in the dorsal subcutaneous tissue of rats. Onyx was not degraded in vivo (Fig. 4f and g). Third, hematoxylin and eosin (H&E) staining was used to study the tissues that were adjacent to the implanted samples. In the PLA/LM hydrogel (red arrow) group, there was a mild acute inflammatory infiltration containing neutrophils (green triangle) and macrophages (yellow triangle) on day 14, and the number of inflammatory cells was significantly reduced on day 28, indicating a reduced inflammatory reaction. Moreover, no necrosis was observed in skin or muscle tissues. By contrast, the tissue around Onyx exhibited a continuous increase in inflammatory cells, including neutrophils (green triangles) and macrophages (yellow triangles), from day 14–28, suggesting a persistent inflammatory reaction. These observations demonstrated that the PLA/LM hydrogel elicited a less pronounced inflammatory response than Onyx (Fig. 4h and S5). Finally, H&E staining of other vital organs (e.g., the heart, brain, liver, lung, spleen, testis, and kidney) showed no significant differences between experimental and control rats, indicating that these embolic agents did not cause systemic response syndrome (Fig. S6). These results demonstrate good biocompatibility and biodegradation of the PLA/LM/DES solution and its-derived PLA/LM hydrogel, allowing it to be used as a liquid embolic agent.

### 3.4. Kidney embolic performances of the PLA/LM/DES and Onyx

The kidney embolic performance of the PLA/LM/DES and Onyx embolic agents in New Zealand rabbit models was compared to evaluate

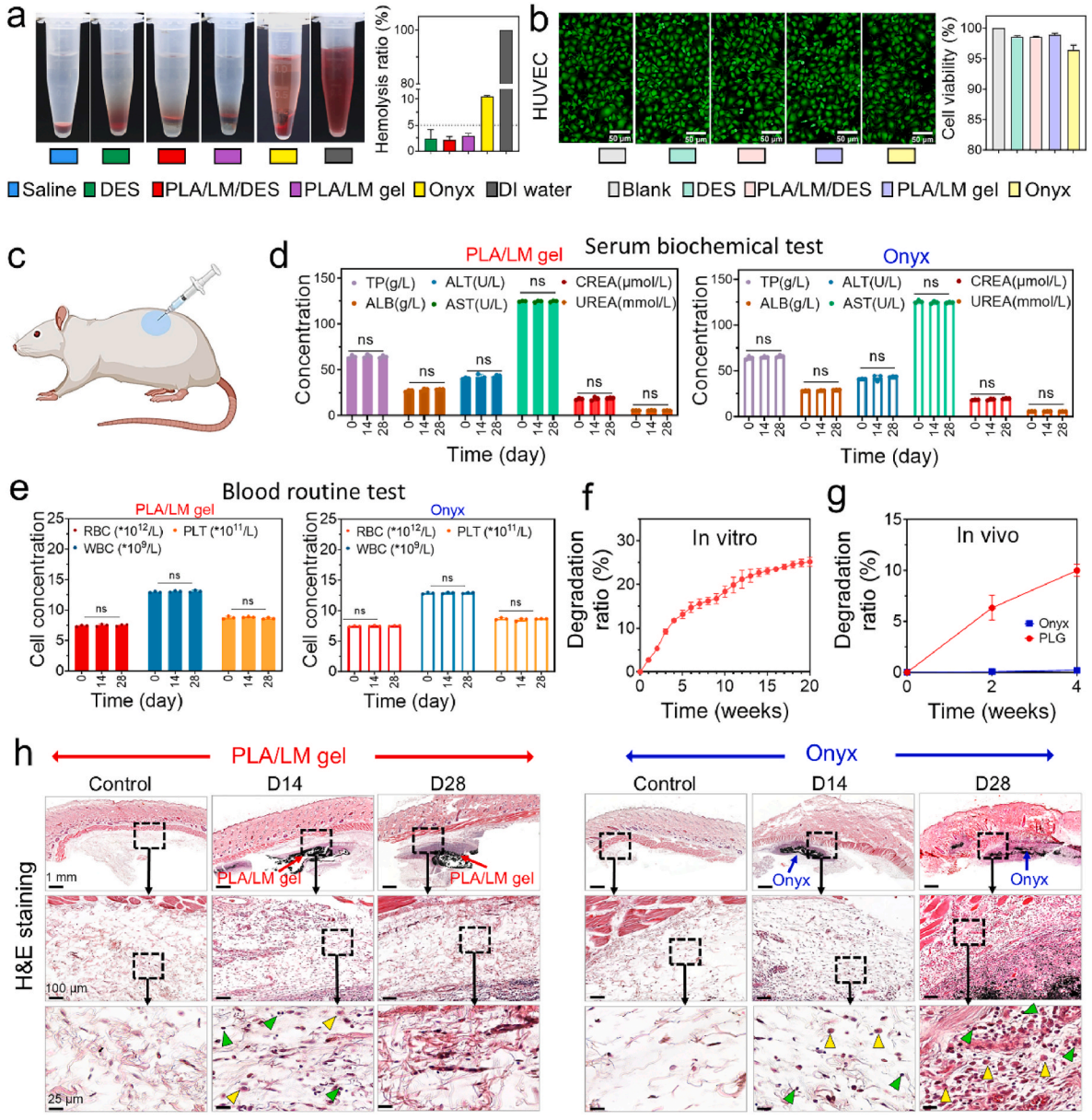


**Fig. 4.** Biocompatibility and biodegradability of the PLA/LM/DES and Onyx embolic agents. (a) Photographs of hemolysis (left) and hemolysis ratios (right) of physiological saline, DES, PLA/LM/DES, PLA/LM gel, Onyx, and deionized water (37 °C, incubation time = 24 h), $n = 3$. (b) Live/dead staining images (left) and cell viability (right) of HUVEC after coincubation with the blank media, DES, PLA/LM/DES, PLA/LM gel, or Onyx for 24 h, $n = 3$. (c) Schematic for injecting liquid embolic agents into the back of a rat. (d, e) Serum biochemical (d) and blood routine tests (e) of rats before and after subcutaneous implantation of PLA/LM/DES or Onyx. Rats, $n = 3$. RBC: red blood cell; WBC: white blood cell; PLT: platelets; TP: total protein; ALB: albumin; ALT: alanine aminotransferase; AST: aspartate aminotransferase; CREA: creatinine; BUN: blood urea nitrogen. (f, g) In vitro (f) and in vivo (g) degradation of the PLA/LM gel or Onyx. (h) Hematoxylin and eosin (H&E) staining (original magnification × 2, × 20, × 80) images of the control tissue and tissue adjacent to PLA/LM gel or Onyx. Green and yellow triangles indicate neutrophils and macrophages, respectively. Data shown are mean ± SD. Statistical significance was analyzed using one-way ANOVA. ns, not significant.

their embolic efficiency and safety (Fig. 5a). Superselective insertion of a 2.7-F microcatheter into the right renal artery via the femoral artery approach and injecting of 0.5 mL iohexol (contrast agent) into the renal artery (white arrow) to confirm patency of the renal artery using digital subtraction angiography (DSA). Then, 0.1–0.2 mL of PLA/LM/DES solution or Onyx was deployed into the right renal artery and its branches under X-ray fluoroscopy monitoring (Video S1). Upon contact with blood, the surface of the PLA/LM/DES underwent gelation instantly and formed a plug with the tip of the catheter, preventing the inside solution from being washed away before complete gelation. The inside solution was then pushed into the branches and underwent gradual gelation via solvent exchange, achieving effective embolization of the right renal artery and its small branches. Finally, iohexol was injected into the bilateral renal arteries to confirm embolization of the right renal artery (Fig. 5b). We monitored the glycerol concentration in the blood. The glycerol in the blood rapidly increased to 0.20 mM in the first 0.5 h, and then decreased to 0 at 3.5 h, indicating that the blood glycerol levels were maintained well below the danger level throughout the process (Fig. S7) [31–33].

After 14 and 28 days of embolization, the PLA/LM hydrogel- and Onyx-embolized kidneys were reexamined using nonenhanced computed tomography (NECT), computed tomography angiography (CTA), color Doppler flow imaging (CDFI), and contrast-enhanced ultrasound (CEUS) imaging techniques (Fig. 5c). NECT and CTA scanning images demonstrated that the PLA/LM hydrogel (red dotted circle) and Onyx (cyan dotted circle) remained stable in the right kidney without

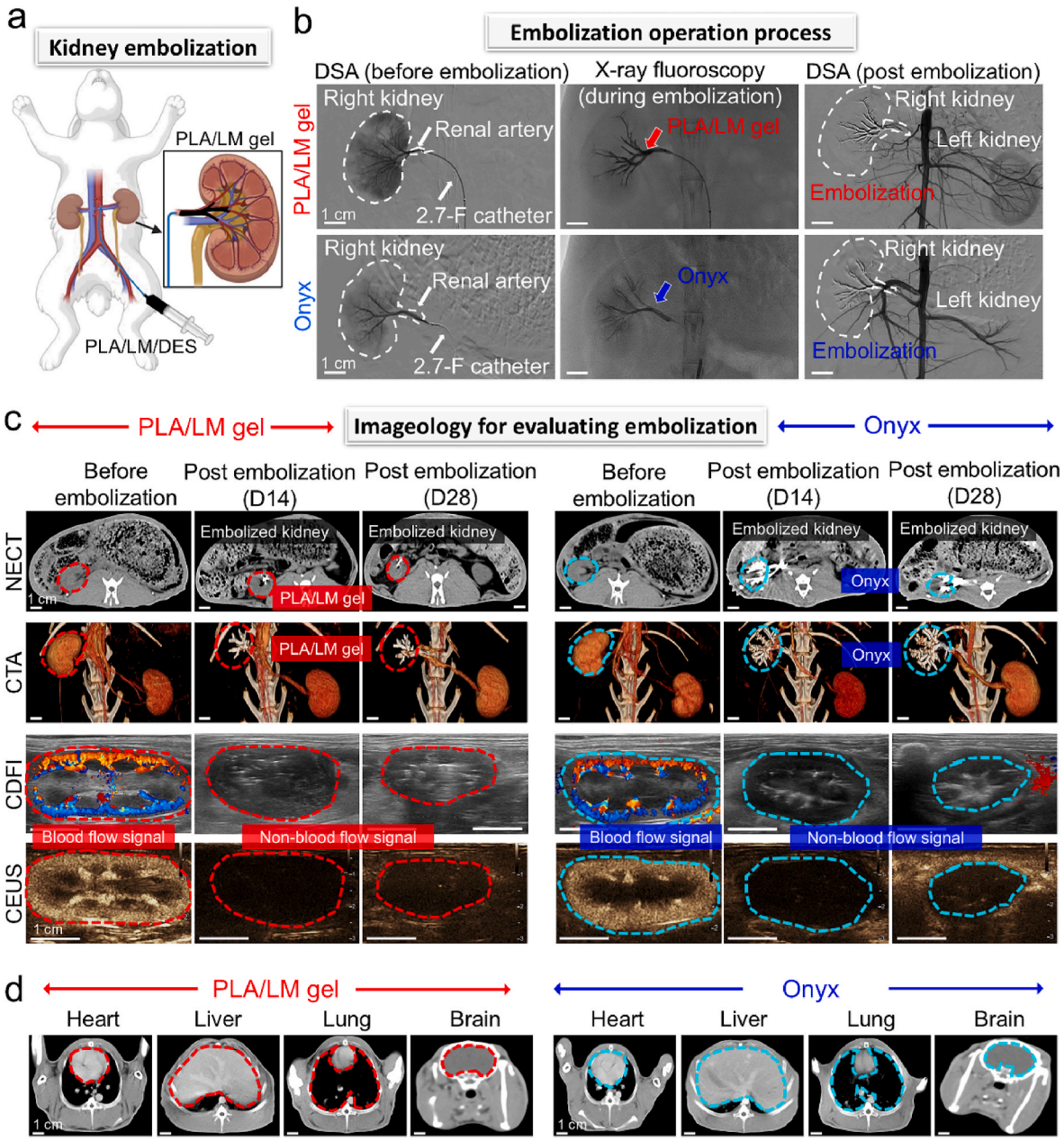


**Fig. 5.** Kidney embolization using PLA/LM/DES and Onyx in a rabbit model. (a) Schematic of kidney embolization. (b) DSA images of the kidney (white dotted circle) before and post embolization, X-ray fluoroscopy image of the PLA/LM gel or Onyx (red or blue arrow) in the embolized kidney. (c) NECT, CTA, CDFI, CEUS images of the embolized kidney before and after embolization at 14 and 28 days. Red and cyan dotted outline represent the kidney embolized with PLA/LM gel and Onyx, respectively. (d) CT scanning images of other vital organs including the brain, heart, liver, and lung in the rabbit whose kidney was embolized with PLA/LM gel or Onyx.

any fragmentation or migration. Simultaneously, these images indicated that the PLA/LM hydrogel could be clearly visualized during or post embolization, which can avoid ectopic embolism. Moreover, CDFI and CEUS images showed no blood flow signal in the embolized kidneys, accompanied by gradual shrinkage in kidney volume (Fig. 5c, Videos S2 and S3). These results highlighted that the renal artery and its branches can be embolized using the PLA/LM/DES-derived hydrogel without recanalization. Furthermore, the embolic efficiency of the PLA/LM/DES-derived hydrogel was similar to that of the commercial embolic agent Onyx. In addition, the systemic effects in rabbits embolized with PLA/LM hydrogel and Onyx were assessed using CECT scans. No apparent abnormal density or structural changes were observed in vital organs including the brain, heart, liver, and lungs on day 27, suggesting that these embolic agents did not enter the microcirculation to induce ectopic embolism (Fig. 5d).

Next, the bilateral kidneys were collected and studied with pathological analyses. The embolized kidney showed significant atrophy, and the other kidneys showed compensatory enlargement on days 14 and 28. The weight of the embolized kidneys gradually decreased (Fig. 6a and S8). Moreover, H&E staining was used to examine the renal parenchyma before and post embolization. After 14 days of embolization using the PLA/LM hydrogel or Onyx, although the renal glomerulus (blue dotted outline) and tubules (blue triangle) maintained their structure, the number of nuclei significantly decreased owing to ischemia. Subsequently, the glomeruli and renal tubules gradually atrophied until extensive coagulative necrosis appeared on day 28. While the non-embolized contralateral kidney showed compensatory hyperplasia, the renal glomerulus enlarged (green dotted outline), and the tubules

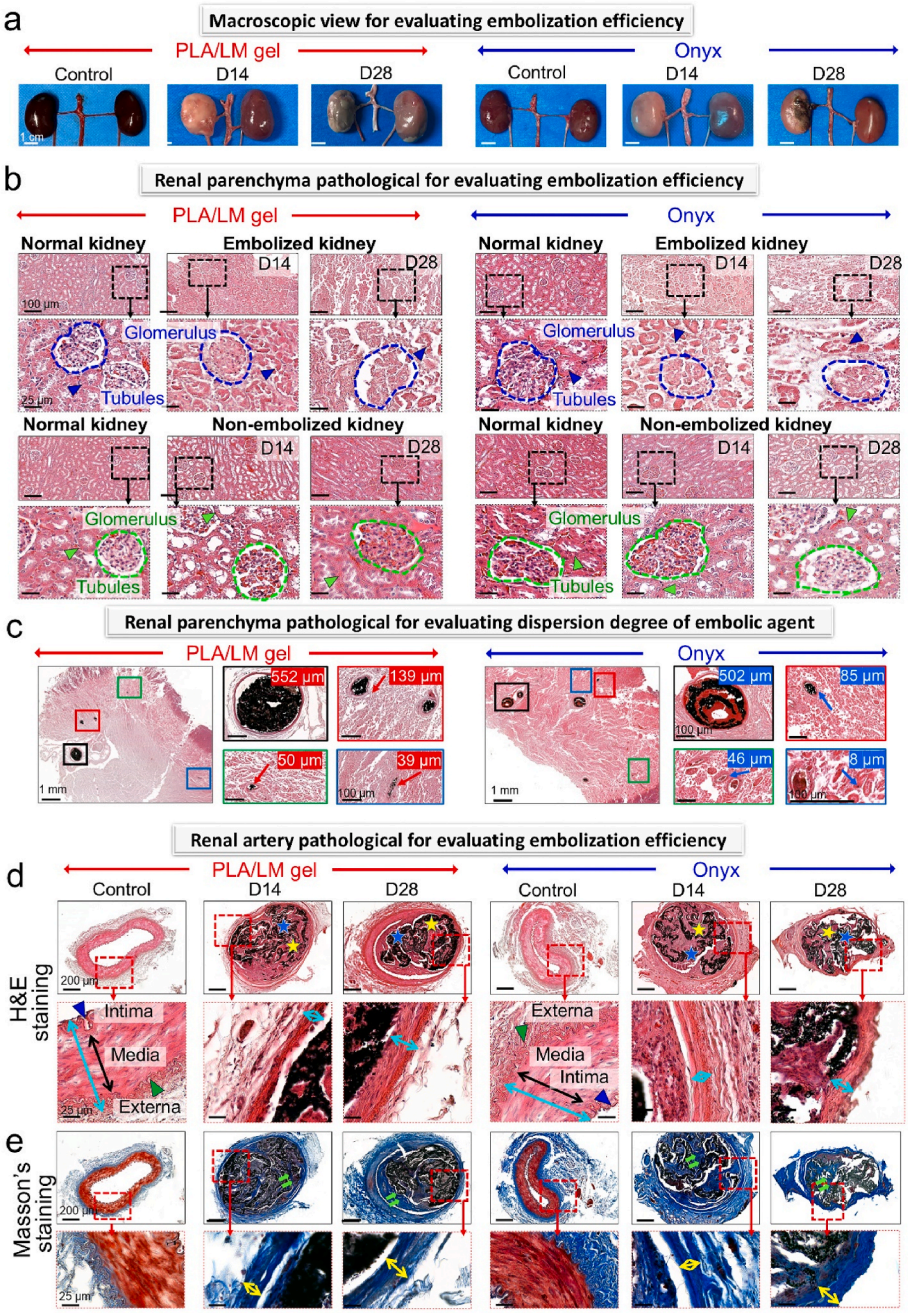


**Fig. 6.** Histopathological evaluation of normal and embolized renal arteries. (a) Photographs of bilateral kidneys before and after embolization at pre-set time. (b) H&E staining images of the renal parenchyma of normal and embolized kidneys (original magnification × 20, × 80). Triangle and dotted outline indicate the renal tubules and glomerular, respectively. (c) H&E staining images of blood vessels in parenchyma. (d) H&E staining images of normal and embolized renal arteries (original magnification × 10, × 80). Blue triangle, black double arrow, green triangle, and cyan double arrow indicate the arterial intima, arterial media, arterial externa, and whole layer of artery, respectively. Blue and yellow star indicate PLA/LM gel or Onyx and thrombus, respectively. (e) Masson's staining images of normal and embolized renal arteries (original magnification × 10, × 80). Yellow double arrow and green arrow indicate collagen fibers in the arterial wall and arterial lumen, respectively.

dilated (green triangle) (Fig. 6b). Furthermore, the degree of dispersion of embolic agents in the renal parenchyma was evaluated (Fig. 6c). PLA/LM gel entered the blood vessels with diameters ranging from 39 to 552 μm (red arrow), while Onyx can diffuse to 8 μm small blood vessels. Such a small vascular arrival point indicated that the embolic agent poses the risk of being washed away by blood flow to other organs, causing an ectopic embolism [34–36].

Next, cross sections of the renal artery were stained using H&E (Fig. 6d). The normal renal artery displayed a clear lumen, arterial intima (blue triangle), arterial media (black double arrow), and arterial externa (green triangle). After embolization using the PLA/LM hydrogel for 14 and 28 days, the lumen of the renal artery was filled with a thrombus (yellow star) and PLA/LM hydrogels (blue star). Simultaneously, the arterial intima and arterial externa gradually disappeared, and the thickness of the arterial media decreased over time owing to the ischemia of the arterial wall. Moreover, the thickness of the arterial wall (cyan double arrow) decreased from days 0–14 and then increased from days 14–28 (Fig. S9). These changes may be attributed to the destruction of the arterial wall in the early stage and proliferation of collagen fibers in the later stage, as confirmed by Masson's staining. The arterial wall

was gradually replaced by collagen fibers (yellow double arrow), and the thickness of the collagen fibers increased (Fig. 6e and S10). Thus, the increased total thickness of the renal arterial wall in later stages may be caused by the deposition of collagen fibers. Massive collagen fibers were observed in the lumen of the embolized renal artery (green arrows). The destruction and fibrotic remodeling of the embolized renal artery suggested that the PLA/LM hydrogel can permanently embolize blood vessels, eliminating the risk of vascular recanalization over time. Finally, body weight, routine blood and serum biochemical tests, and vital organs between normal and experimental rabbits demonstrated no significant differences, indicating the safety of PLA/LM/DES as a liquid embolic agent (Fig. S11–S13).

In general, the PLA/LM/DES-derived hydrogel not only exhibited effective, permanent, and safe embolization of the renal artery and its smaller branches but also guaranteed clear visibility via X-rays during and after embolization.

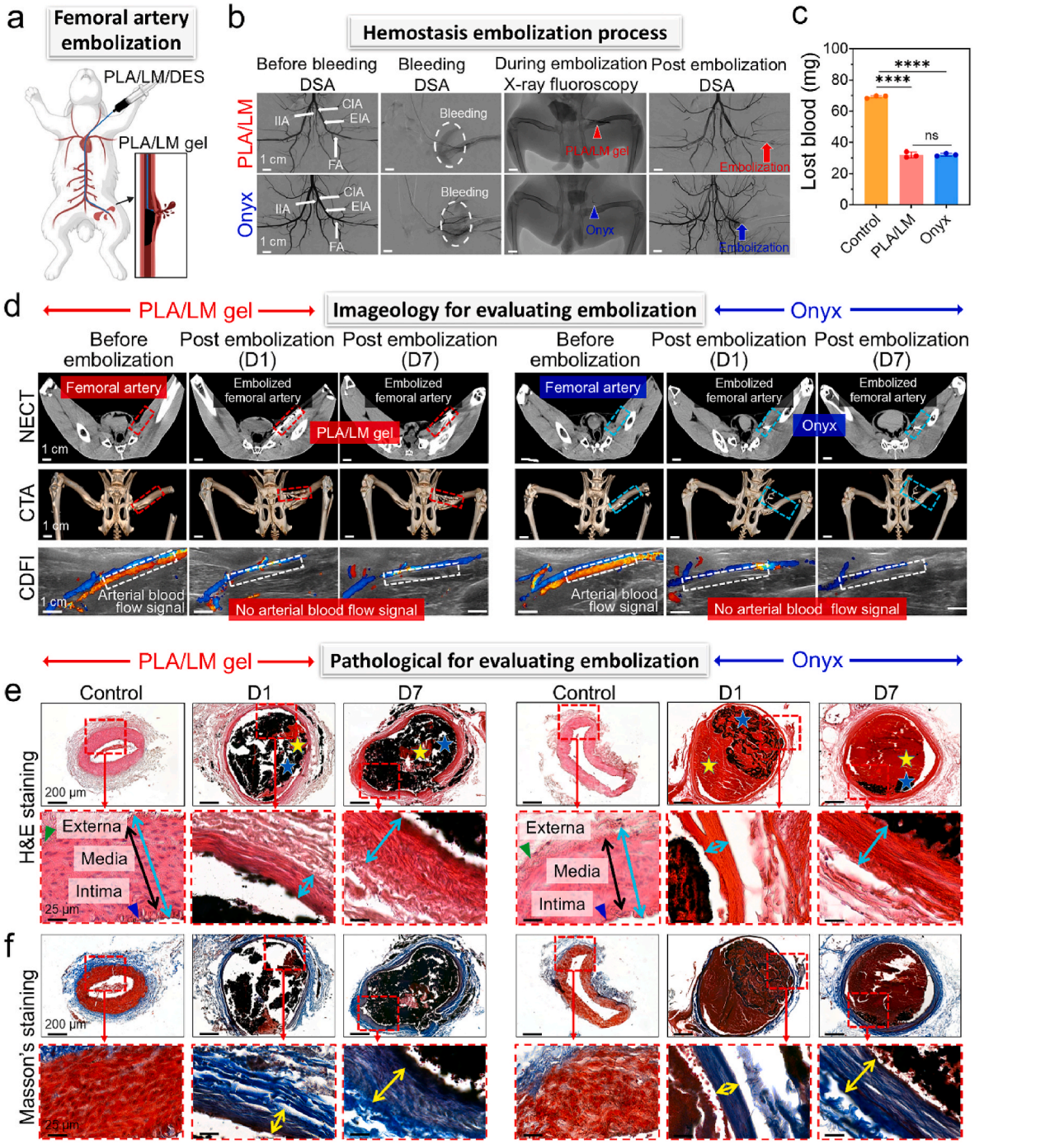


**Fig. 7.** Ruptured FA embolic performance of PLA/LM hydrogel or Onyx in a rabbit model. (a) Schematic of ruptured FA embolization. (b) DSA images of the CIA, EIA, IIA, and FA before and after embolization. X-ray fluoroscopy image of PLA/LM hydrogel (red arrow) or Onyx (blue arrow) during embolization. (c) Lost blood in blank, PLA/LM, and Onyx groups. (d) NECT, CTA, and CDFI images of normal and embolized FA. (e) H&E staining images of normal and embolized FA (original magnification × 10, × 80). Blue triangle, black double arrow, green triangle, and cyan double arrow indicate arterial intima, arterial media, arterial externa and whole layer of artery, respectively. (f) Masson's staining images of normal and embolized FA (original magnification × 10, × 80). Yellow double arrow indicates collagen fiber in the arterial wall. Rabbits, $n = 3$. Data are shown as mean ± SD. Statistical significance was calculated by one-way ANOVA. ns, not significant, ****$p < 0.0001$.

### 3.5. Hemostasis of the PLA/LM/DES and Onyx

We further employed a rabbit femoral artery (FA) puncture bleeding model to demonstrate the embolic efficiency of the PLA/LM/DES (Fig. 7a). Inserting a 2.7-F microcatheter into the FA via the transcarotid approach, and injecting iohexol to confirm the patency of the common iliac artery (CIA), external iliac artery (EIA), internal iliac artery (IIA), and FA. Then, the FA was punctured, which can be confirmed in DSA images (Video S4). Immediately, 0.3 mL PLA/LM/DES solution (red triangle) was slowly deployed into the bleeding point to stop the bleeding, resulting in invisible FA (red arrow) and less lost blood (Fig. 7b−c and Video S5). Moreover, the lost blood in the PLA/LM/DES and Onyx groups was not significantly different. In addition, the concentration of glycerol in the blood was always within the safe range and decreased to zero within 3.5 h (Fig. S14).

The treatment sites were re-examined on days 1 and 7 post embolization. NECT and CTA images showed that the PLA/LM gel (red dotted outline) remained stable in FA without fragmentation or migration. The CDFI images showed no blood flow signal in the embolized FA (white dotted outline). These results demonstrated that the PLA/LM gel could effectively embolize ruptured FA without vascular rebleeding and recanalization (Fig. 7d, Videos S6 and S7).

Next, cross-sections of the FA were studied using H&E and Masson's staining (Fig. 7e and f). Normal FA exhibited a clear lumen, arterial intima (blue triangle), arterial media (black double arrow), and arterial externa (green triangle). After embolization, the lumen of the FA was filled with thrombus (yellow star), PLA/LM gel, or Onyx (blue star). Meanwhile, the arterial intima and arterial externa gradually disappeared, and the thickness of the arterial media decreased over time owing to the ischemia of the arterial wall (Figs. S15–16). Moreover, the total thickness of the entire FA wall decreased from day 0 to day 1 and then increased from day 1 to day 7, which could be attributed to the destruction of the arterial wall in the early stage and the proliferation of collagen fibers (yellow double arrow). Notably, the Onyx-embolized lumen contained more thrombi than the PLA/LM gel group. In addition, after embolization with the PLA/LM gel, there were no other systematic effects on the rabbits, indicating its safety as a liquid embolic agent (Figs. S17–19). These results indicated that the PLA/LM hydrogel could permanently embolize blood vessels, eliminating the risk of vascular recanalization over time.

## 4. Discussion

First, we selected Gly as the hydrogen-bond donor and ChCl as the hydrogen-bond acceptor to prepare DES. ChCl, one of the most common hydrogen-bond acceptor, is a nutrient similar to vitamin B, whereas Gly is a Food and Drug Administration (FDA)-approved inactive ingredient that can be used in formulating intravenous injection preparations. Moreover, among DES solutions prepared with different ratios of ChCl to Gly, the sample with a 1:3 ratio demonstrated the highest solubility (0.2 g/mL) in PLA. Dissolving a large amount of PLA can facilitate rapid gelation and embolization; therefore, we chose this ratio. In addition, DES and its constituent components are highly hygroscopic; therefore, throughout the preparation and storage processes, these samples should be kept in a sealed container.

For the contrast agent, the addition of tantalum (Ta) powder to PLA/DES can obtain a stable PLA/Ta/DES gel, which could not be then injected through the microcatheter (Fig. S20). Thus, LM, with excellent fluidity and biocompatibility, was used as a contrast agent. The LM used in this study was an alloy composed of Ga (68.5 %), In (21.5 %), and Sn (10 %). Its toxicity is closely associated with the properties of Ga, In, and Sn. Ga exhibits very low toxicity and serves as an effective immunosuppressant, making it clinically acceptable for disease treatment. In has relatively low toxicity; however, caution should be exercised regarding the potential health risks associated with high-dose exposure. Sn and its simple derivatives are generally nontoxic. Nonetheless, excessive ingestion or inhalation of Sn can result in adverse symptoms, including dizziness, diarrhea, nausea, chest tightness, shortness of breath, and dry mouth. Therefore, the toxicity of LM is dose-dependent [37,38]. Moreover, the form of LM significantly affects its toxicity. LMs are generally safe for use in solution; however, when large amounts of free ions are released, their toxicity increases considerably. In our study, the LM was embedded in a PLA hydrogel network, which can help prevent LM leakage and associated risks. Throughout the four-week experimental period, the rats and rabbits remained healthy and showed an increase in body weight. Additionally, typical liver function markers, including alanine aminotransferase (ALT) and aspartate aminotransferase (AST), and kidney function markers, including creatinine (CREA) and urea (UREA), did not increase over the four weeks. H&E staining of other vital organs (e.g., the heart, brain, liver, lung, spleen, testis, and kidney) revealed no significant differences between the experimental and blank groups (Fig. 4d and e, S6, S11, S12, S13, S18, and S19) [39]. These results suggest that LM embedded in PLA hydrogel networks exhibit low toxicity in vivo. Additionally, we plan to investigate the embolic performance, safety, and biodegradation of PLA/LM/DES embolic agent in large animal models (such as pigs and dogs) for an increased duration, such as 1–2 years, in a follow-up study.

The difference in inflammation between Onyx and PLA/LM/DES can be explained as follows: 1) The DMSO in Onyx has a strong stimulatory effect on tissues and is likely to induce a stronger inflammatory response [40]. By contrast, DES has improved biocompatibility and does not cause a strong stimulatory effect on tissues. 2) The non-degradable ethylene vinyl alcohol (EVOH) polymer in Onyx can lead to sustained activation of immune cells, which release proinflammatory cytokines, thereby triggering a stronger inflammatory response. By contrast, PLA is biodegradable, and its degradation products are coenzymes in the body, resulting in a milder inflammatory response [41]. Furthermore, the difference in embolization performance between Onyx and PLA/DES can be explained as follows. After Onyx undergoes solvent exchange with water, it forms loose precipitates with weak mechanical properties that are easily washed away by blood flow. By contrast, when PLA/LM/DES undergoes solvent exchange with water, it transforms into a continuous PLA/LM hydrogel with good mechanical properties, allowing it to effectively resist removal by blood flow (Fig. 3j). This behavior leads to risks in Onyx-embolized patients. For instance, some cases of recanalization, recurrence, and even death have been reported after Onyx embolization in a rabbit animal model [42,43].

## 5. Conclusion

We present an innovative and biocompatible liquid embolic agent composed of a coenzyme-based polymer (PLA), a green and biocompatible solvent (DES), and a biocompatible contrast agent (LM NPs). Owing to the strong hydrogen bonding between PLA and DES, DES not only was used as a green and biocompatible alternative to conventional organic solvents (such as DMSO and ethanol) to dissolve PLA, but also can prevent depolymerization of the PLA. After introducing PLA/DES/LM into water, most of the DES was replaced with water molecules, whereas some ChCl remained integrated within the PLA through strong hydrogen bonding. This hydrogen bonding prevented PLA depolymerization and enhanced the PLA network, resulting in the formation of a stable PLA hydrogel rather than yielding depolymerized LA monomers. Moreover, the electrostatic interactions between PLA and LM NPs can further enhance the hydrogel network, leading to the formation of a stable PLA/LM hydrogel with excellent mechanical properties. PLA/LM/DES showed better mechanical properties, better in vitro hemocompatibility and cytocompatibility, and milder in vivo inflammatory response than the DMSO-containing commercial embolic agent Onyx. In the animal experiments, when PLA/LM/DES was injected into the targeted blood vessel, it underwent gelation from the outer layer to the inside via gradual solvent exchange, which allowed the PLA/LM/DES to be pushed forward into the small branches via blood pressure and

injection force. In rabbit renal artery and ruptured FA models, PLA/LM/DES showed more effective and safer embolization than Onyx. Owing to its easy preparation, good biocompatibility, and effective and safe embolization performance, PLA/LM/DES liquid embolic agent is a potential candidate for a new embolic agent.

## CRediT authorship contribution statement

**Yitong Zhou:** Writing – review & editing, Writing – original draft, Methodology, Investigation, Data curation, Conceptualization. **Menghui Liu:** Methodology, Data curation. **Chuandong He:** Methodology, Investigation. **Jiayuan Lin:** Methodology. **Yanlv Chen:** Methodology, Formal analysis. **Mingyu Yu:** Methodology. **Yuhan Jiang:** Investigation. **Xin Peng:** Writing – review & editing, Writing – original draft, Visualization, Supervision, Funding acquisition.

## Data Availability Statement

The data that support the findings of this study are available from the corresponding author upon reasonable request.

## Ethics approval and consent to participate

All the experiments complied with the animal ethics guidelines of the Animal Ethics Committee of the Fifth Affiliated Hospital of Sun Yat-sen University (IAC24W123).

## Declaration of competing interest

The authors declare that they have no conflict of interest.

## Acknowledgements

Yitong Zhou and Menghui Liu contributed equally to this work. The authors acknowledge grants from the National Natural Science Foundation of China (22205264), the Guangdong-Hong Kong-Macao University Joint Laboratory of Interventional Medicine Foundation of Guangdong Province (2023LSYS001), and the Hundred Talents Program of Sun Yat-sen University. The part of the schematic diagrams in Fig. 1c, 4c, 5a and 7a are created with BioRender.com.

## Appendix A. Supplementary data

Supplementary data to this article can be found online at https://doi.org/10.1016/j.bioactmat.2025.02.037.

## References

[1] J. Hu, H. Albadawi, B.W. Chong, A.R. Deipolyi, R.A. Sheth, A. Khademhosseini, R. Oklu, Advances in biomaterials and technologies for vascular embolization, Adv. Mater. 31 (33) (2019) e1901071.
[2] G. Ko, J.W. Choi, N. Lee, D. Kim, T. Hyeon, H.C. Kim, Recent progress in liquid embolic agents, Biomaterials 287 (2022) 121634.
[3] J. Hu, H. Albadawi, Z. Zhang, M.A. Salomao, S. Gunduz, S. Rehman, L. D'Amone, J. L. Mayer, F. Omenetto, R. Oklu, Silk embolic material for catheter-directed endovascular drug delivery, Adv. Mater. 34 (2) (2022) e2106865.
[4] J. Hu, I. Altun, Z. Zhang, H. Albadawi, M.A. Salomao, J.L. Mayer, L. Hemachandra, S. Rehman, R. Oklu, Bioactive-tissue-derived nanocomposite hydrogel for permanent arterial embolization and enhanced vascular healing, Adv. Mater. 32 (33) (2020) e2002611.
[5] I. Altun, J. Hu, H. Albadawi, Z. Zhang, M.A. Salomao, J.L. Mayer, L. Jamal, R. Oklu, Blood-derived biomaterial for catheter-directed arterial embolization, Adv. Mater. 32 (52) (2020) 2005603.
[6] R.K. Avery, H. Albadawi, M. Akbari, Y.S. Zhang, M.J. Duggan, D.V. Sahani, B. D. Olsen, A. Khademhosseini, R. Oklu, An injectable shear-thinning biomaterial for endovascular embolization, Sci. Transl. Med. 8 (365) (2016), 365ra156-365ra156.
[7] M. Liu, Y. Sun, Y. Zhou, Y. Chen, M. Yu, L. Li, L. Yan, Y. Yuan, J. Chen, K. Zhou, H. Shan, X. Peng, A novel coacervate embolic agent for tumor chemoembolization, Adv. Health. Mater. 13 (19) (2024) 2304488.
[8] M. Liu, Y. Wang, Y. Chen, L. Li, Y. Sun, Y. Li, Y. Yuan, P. Lu, W. Zhang, P. Pang, X. Peng, H. Shan, Solvent exchange induced in situ formed hydrogel as liquid embolic agents, Adv. Funct. Mater. 33 (45) (2023) 2305153.
[9] Q.W. Dongdong Jin, Kai Fung Chan, Neng Xia, Q.W. Haojin Yang, Simon Chun Ho Yu, L. Zhang, Swarming self-adhesive microgels enabled aneurysm on-demand embolization in physiological blood flow, Sci. Adv. 9 (2023) eadf9278.
[10] Q. Wang, Y. He, M. Shen, L. Huang, L. Ding, J. Hu, Y. Dong, H. Fu, Q. Wang, Y. Sun, L. Zhang, J. Cao, Y. Duan, Precision embolism: biocompatible temperature-sensitive hydrogels as novel embolic materials for both mainstream and peripheral vessels, Adv. Funct. Mater. 31 (20) (2021) 2011170.
[11] J. Lim, G. Choi, K.I. Joo, H.J. Cha, J. Kim, Embolization of vascular malformations via in situ photocrosslinking of mechanically reinforced alginate microfibers using an optical-fiber-integrated microfluidic device, Adv. Mater. 33 (14) (2021) e2006759.
[12] S.W. Jacob, R. Herschler, Pharmacology of DMSO, Cryobiology 23 (1) (1986) 14–27.
[13] S. Wray, R.D. Smith, Mechanisms of action of pH-induced effects on vascular smooth muscle, Mol. Cell. Bioch. 263 (1) (2004) 163–172.
[14] B.B. Hansen, S. Spittle, B. Chen, D. Poe, Y. Zhang, J.M. Klein, A. Horton, L. Adhikari, T. Zelovich, B.W. Doherty, B. Gurkan, E.J. Maginn, A. Ragauskas, M. Dadmun, T.A. Zawodzinski, G.A. Baker, M.E. Tuckerman, R.F. Savinell, J. R. Sangoro, Deep eutectic solvents: a review of fundamentals and applications, Chem. Rev. 121 (3) (2021) 1232–1285.
[15] P. Cysewski, T. Jeliński, M. Przybyłek, A. Mai, J. Kułak, Experimental and machine-learning-assisted design of pharmaceutically acceptable deep eutectic solvents for the solubility improvement of non-selective cox inhibitors ibuprofen and ketoprofen, Molecules 29 (10) (2024) 2296.
[16] S. Ahmed Shahani, H. Warsi Khan, A. Mohd Shaiff, M. Goto, M. Moniruzzaman, Screening of ionic liquids for the solubility enhancement of quinine using COSMO-RS, J. Mol. Liq. 409 (2024) 125388.
[17] P. Cysewski, T. Jeliński, M. Przybyłek, Exploration of the solubility hyperspace of selected active pharmaceutical ingredients in choline- and betaine-based deep eutectic solvents: machine learning modeling and experimental validation, Molecules 29 (20) (2024) 4894.
[18] Y. Mu, T. Dai, J. Fan, Y. Cheng, Prediction of acetylene solubility by a mechanism-data hybrid-driven machine learning model constructed based on COSMO-RS theory, J. Mol. Liq. 414 (2024) 126194.
[19] R. Cabezas, D. González-Revuelta, E. Zurob, F. Olea, E. Quijada-Maldonado, D. Gorri, PEBAX polymer inclusion hydrophobic deep eutectic solvent membranes for pervaporation of biobutanol: mass transfer and COSMO-RS analysis, J. Mol. Liq. 395 (2024) 123909.
[20] P. Cysewski, T. Jeliński, M. Przybyłek, Intermolecular interactions of edaravone in aqueous solutions of ethaline and glyceline inferred from experiments and quantum chemistry computations, Molecules 28 (2) (2023) 629.
[21] C. Li, X. Liu, H. Ke, H. Wang, J. Xu, C. Zhang, Enhancement of clozapine solubility in three aqueous choline chloride-based deep eutectic solvents: experimental and COSMO-RS prediction, J. Mol. Liq. 359 (2022) 119298.
[22] Q. Zhang, C.Y. Shi, D.H. Qu, Y.T. Long, B.L. Feringa, H. Tian, Exploring a naturally tailored small molecule for stretchable, self-healing, and adhesive supramolecular polymers, Sci. Adv. 4 (7) (2018) eaat8192.
[23] Y. Dai, G.J. Witkamp, R. Verpoorte, Y.H. Choi, Natural deep eutectic solvents as a new extraction media for phenolic metabolites in Carthamus tinctorius L, Anal. Chem. 85 (13) (2013) 6272–6278.
[24] X. Chen, J. Jiang, J. Zhu, W. Song, C. Liu, L.P. Xiao, Deep eutectic solvent with Lewis acid for highly efficient biohydrogen production from corn straw, Bioresour. Technol. 362 (2022) 127788.
[25] J.D. Mota-Morales, R.J. Sánchez-Leija, A. Carranza, J.A. Pojman, F. del Monte, G. Luna-Bárcenas, Free-radical polymerizations of and in deep eutectic solvents: green synthesis of functional materials, Prog. Polym. Sci. 78 (2018) 139–153.
[26] Y. Wang, S. Sun, P. Wu, Adaptive ionogel paint from room-temperature autonomous polymerization of α-thioctic acid for stretchable and healable electronics, Adv. Funct. Mater. 31 (24) (2021) 202101494.
[27] C. Cui, L. Mei, D. Wang, P. Jia, Q. Zhou, W. Liu, A self-stabilized and water-responsive deliverable coenzyme-based polymer binary elastomer adhesive patch for treating oral ulcer, Nat. Commun. 14 (1) (2023) 7707.
[28] X. Peng, Y. Li, T. Li, Y. Li, Y. Deng, X. Xie, Y. Wang, G. Li, L. Bian, Coacervate-derived hydrogel with effective water repulsion and robust underwater bioadhesion promotes wound healing, Adv. Sci. 9 (31) (2022) 2203890.
[29] X. Peng, Y. Li, M. Liu, Z. Li, X. Wang, K. Zhang, X. Zhao, G. Li, L. Bian, Complex coacervate-derived hydrogel with asymmetric and reversible wet bioadhesion for preventing UV light-induced morbidities, Bioact. Mater. 30 (2023) 62–72.
[30] W. Rungseevijitprapa, R. Bodmeier, Injectability of biodegradable in situ forming microparticle systems (ISM), Eur. J. Pharm. Sci. 36 (4–5) (2009) 524–531.
[31] P. Montner, D.M. Stark, M.L. Riedesel, G. Murata, R. Robergs, M. Timms, T. W. Chick, Pre-exercise glycerol hydration improves cycling endurance time, Int. J. Sports Med. 17 (1) (1996) 27–33.
[32] R.A. Robergs, S.E. Griffin, Glycerol. biochemistry, pharmacokinetics and clinical and practical applications, Sports Med. 26 (3) (1998) 145–167.
[33] S.P. van Rosendal, M.A. Osborne, R.G. Fassett, J.S. Coombes, Physiological and performance effects of glycerol hyperhydration and rehydration, Nutr. Rev. 67 (12) (2009) 690–705.
[34] S.K. Natarajan, B. Ghodke, G.W. Britz, D.E. Born, L.N. Sekhar, Multimodality treatment of brain arteriovenous malformations with microsurgery after embolization with onyx: single-center experience and technical nuances, Neurosurgery 62 (6) (2008) 1213–1225. ; discussion 1225-6.

[35] Y. Jiang, Y. Zhang, Z. Lu, X. Wang, S. Bai, Y. Chen, J. Mao, G. Liu, Liquid embolic agents for interventional embolization, Chem. Phys. Mater. 1 (1) (2022) 39–50.
[36] M. Saeed Kilani, J. Izaaryene, F. Cohen, A. Varoquaux, J.Y. Gaubert, G. Louis, A. Jacquier, J.M. Bartoli, G. Moulin, V. Vidal, Ethylene vinyl alcohol copolymer (Onyx®) in peripheral interventional radiology: indications, advantages and limitations, Diagn. Interv. Imag. 96 (4) (2015) 319–326.
[37] S. Chen, R. Zhao, X. Sun, H. Wang, L. Li, J. Liu, Toxicity and biocompatibility of liquid metals, Adv. Healthc. Mater. 12 (3) (2023) 2201924.
[38] J. Yan, Y. Lu, G. Chen, M. Yang, Z. Gu, Advances in liquid metals for biomedical applications, Chem. Soc. Rev. 47 (8) (2018) 2518–2533.
[39] L. Fan, M. Duan, Z. Xie, K. Pan, X. Wang, X. Sun, Q. Wang, W. Rao, J. Liu, Injectable and radiopaque liquid metal/calcium alginate hydrogels for endovascular embolization and tumor embolotherapy, Small 16 (2) (2020) 1903421.
[40] S.-H. Huang, C.-H. Wu, S.-J. Chen, H.-K. Sytwu, G.-J. Lin, Immunomodulatory effects and potential clinical applications of dimethyl sulfoxide, Immunobiology 225 (3) (2020) 151906.
[41] T. Khodaei, E. Schmitzer, A.P. Suresh, A.P. Acharya, Immune response differences in degradable and non-degradable alloy implants, Bioact. Mater. 24 (2023) 153–170.
[42] R. Thiex, I. Wu, J.B. Mulliken, A.K. Greene, R. Rahbar, D.B. Orbach, Safety and clinical efficacy of Onyx for embolization of extracranial head and neck vascular anomalies, Am. J. Neuroradiol. 32 (6) (2011) 1082–1086.
[43] T. Struffert, C. Roth, B. Romeike, I.O. Grunwald, W. Reith, Onyx in an experimental aneurysm model: histological and angiographic results, J. Neurosurg. 109 (1) (2008) 77–82.